Phys. Med. Biol. 39 (1994) 609–618. Printed in the UK

3D brain mapping using a deformable neuroanatomy

Gary E Christensen†, Richard D Rabbitt‡ and Michael I Miller†

† The Institute for Biomedical Computing and The Electronic Signals and Systems Research Laboratory, Washington University, St Louis, MO 63130, USA

‡ Mechanical Engineering Department, Washington University, St Louis, MO 63130, USA

Received 13 October 1993

Abstract. This paper presents two different mathematical methods that can be used separately or in conjunction to accommodate shape variabilities between normal human neuroanatomies. Both methods use a digitized textbook to represent the complex structure of a typical normal neuroanatomy. Probabilistic transformations on the textbook coordinate system are defined to accommodate shape differences between the textbook and images of other normal neuroanatomies. The transformations are constrained to be consistent with the physical properties of deformable elastic solids in the first method and those of viscous fluids in the second. Results presented in this paper demonstrate how a single deformable textbook can be used to accommodate normal shape variability.

1. Introduction

The goal of this research is to provide algorithms for representing normal neuroanatomies by precisely specifying the global anatomical relationships between structures and how they can vary from one individual to another. The method of Grenander's shape models is used to represent the structure and variability of the brain. The structure of a typical normal brain is represented by constructing a neuroanatomy textbook and the shape variability is accommodated by defining probabilistic transformations on the coordinate system of the textbook. By applying the transformations to the textbook, a rich family of brains may be represented using a single textbook. The transformations on the textbook need to maintain the continuity of the textbook, and also be of high spatial dimension to accommodate the complex anatomy of the brain–ventricles, cortical folds, etc. We achieve this by constraining the set of transformations to those consistent with physical deformations of real materials such as elastic solids and viscous fluids.

The neuroanatomy textbook is a registered set of images generated from a typical healthy brain. It consists of two types of image, measured and labelled. The measured set of images can consist of MR images, CT images, digitized photographs of the cryosectioned brain, etc. The labelled images contain information about the measured images, consisting of structure names, sizes, locations, functionality, dependence on other structures, etc. The textbook is individualized by estimating the transformation that accommodates the shape differences in the measured images of the textbook with measured images from a subject's brain. Once this transformation is known, all the information contained in the labelled images of the textbook is mapped onto the measured images of the subject.

Over the last decade, there has been much research in the area of deformable atlases. Methods such as those of Pelizzari *et al* (1989) and Evans *et al* (1991) involve low-dimensional transformations and require that the investigator locate landmarks in the data

0031-9155/94/030609+10$19.50

images that correspond with landmarks in the atlas. Other methods such as those of Bajcsy and Kovacic (1989) and Collins *et al* (1992) use high-dimensional transformations but suffer from small deformation assumptions. The method described in this paper overcomes the limitation of small deformations and does not require human intervention to place landmarks.

2. Anatomical textbook and transformations

The neuroanatomy textbook is a digitized set of images generated from a typical healthy brain. These images show what the textbook brain looks like when measured with different medical instruments. The measured images in the textbook can include MR spin-density, t1, and t2 images, CT attenuation density images, and functional PET images. The textbook also contains symbolic information such as white matter tracts, grey matter nuclei, Broca's areas, etc. The symbolic information is included in the textbook as segmentation images and text strings associated with a location in the textbook. For the work in this paper, we assume that the measured images in the textbook are acquired in register or registered in a preprocessing step. Registration of the textbook modalities can be accomplished in a fashion similar to that described in this paper with one minor change. The likelihood of the deformed textbook and study would have to be changed from an intensity-based function to a function based on common features such as edges.

To make the notion of a textbook more formal, we define the textbook to be a vector mapping of the coordinate system $\Omega \subset \mathcal{R}^3$. The range of the textbook is defined to be $\mathcal{T}$, which is an M-fold product of spaces $\mathcal{T}_1 \times \mathcal{T}_2 \times \cdots \times \mathcal{T}_M$ where each component $T_m \in \mathcal{T}_m$ corresponds to a different image in the textbook. The triple $(\Omega, \boldsymbol{T}, \mathcal{T})$ is termed the anatomical textbook.

There are two kinds of variation that must be accommodated: normal variation between humans and diseased or abnormal states. Diseased and abnormal variation is not addressed in this paper. Focusing on normal human variation, a set of transformations $\boldsymbol{h} \in \mathcal{H}$ on the ideal coordinate system is defined where $\mathcal{H}$ is the set of homeomorphic maps $\boldsymbol{h} : \Omega \rightarrow \Omega$ where

$$\boldsymbol{h} : \boldsymbol{x} = (x_1, x_2, x_3) \rightarrow (x_1 - u_1(\boldsymbol{x}), x_2 - u_2(\boldsymbol{x}), x_3 - u_3(\boldsymbol{x})). \tag{1}$$

The vector field $\boldsymbol{u}(\boldsymbol{x}) = [u_1(\boldsymbol{x}), u_2(\boldsymbol{x}), u_3(\boldsymbol{x})]^{\mathrm{T}}$ is called the displacement field. The maps constructed from these transformations allow for the dilation, contraction, and warping of the coordinate system of the textbook into the coordinate system of the individual anatomy at a very local level. The set of normal anatomies generated from the textbook $(\Omega, \boldsymbol{T}, \mathcal{T})$ becomes $\{\boldsymbol{T} \circ \boldsymbol{h} : \boldsymbol{h} \in \mathcal{H}\}$, with $\circ$ the composition operator.

3. Problem statement

A data set from a subject is represented by a *study* $\boldsymbol{S}$, an N-valued vector function consisting of N characterizing data sets $\{S_n\}_{n=1}^{N}$. It is assumed that each component of the study is present in the textbook, which implies $S_n : \Omega \rightarrow \mathcal{T}_{m_n}$, for some $m_n \in \{1, 2, \ldots, M\}$ and that the study modalities are acquired in register.

Problem statement: find the transformation, $\hat{\boldsymbol{h}} \in \mathcal{H}$ on Ω, that accounts for the shape differences between the textbook, $(\Omega, \boldsymbol{T}, \mathcal{T})$, and the study, $\boldsymbol{S}$, where $\mathcal{H}$ is the set of all allowable transformations.

3.1. Elastic model

A Bayesian approach is adopted to estimate the parameters ξ of the transformation $\hat{h}(x, \xi)$ that satisfies an elastic-solid model (Miller *et al* 1993). In this method, the posterior $p(\xi \mid S)$ is defined in terms of a likelihood $p(S \mid \xi)$ and a prior $p(\xi)$, i.e.

$$p(\xi \mid S) \propto p(S \mid \xi)p(\xi). \tag{2}$$

The textural variability of the data as well as sensor noise is accounted for by defining the likelihood $p(S, \xi)$. We assume the likelihood to be of a Gibbs' form $(1/Z)e^{-H(S,T)}$, where

$$H(S, T) = \frac{1}{2\sigma^2} \int_\Omega \sum_{n=1}^{N} |T_n(h(x)) - S_n(x)|^2 \, dx \tag{3}$$

and T_n and S_n correspond to the same modalities. The form of the potential in (3) is not fixed and can be modified to account for other more appropriate statistical models such as those that are Poisson based.

The prior $p(u)$ is used to ensure that the transformations $h \in \mathcal{H}$ obey the physical properties of elastic solids. In particular, an elastic transformation is smooth and continuous so that structures in the textbook are not broken apart. We assume that the elastic-solid prior has a Gibbs' form $(1/Z)e^{-H(u)}$ with potential energy

$$H(u) = \frac{\alpha}{2} \sum_{i=1}^{3} \sum_{j=1}^{3} \int_\Omega \lambda_0 \left(\frac{\partial u_i(x)}{\partial x_i} \right) \left(\frac{\partial u_j(x)}{\partial x_j} \right) + \frac{\mu_0}{2} \left(\frac{\partial u_i(x)}{\partial x_j} + \frac{\partial u_j(x)}{\partial x_i} \right)^2 dx \tag{4}$$

where λ_0 and μ_0 are the Lamé elasticity constants and α is a Lagrange multiplier. Equation (4) is the sum of the stress times the strain in the three coordinate directions and the three shear planes of Ω.

We parameterize the elastic-solid transformation by expressing it in terms of a complete orthonormal basis such that

$$u(x) = \sum_{i,j,k=0}^{d} \sum_{n=1}^{3} \xi_{n,i,j,k} e_{n,i,j,k}(x) \tag{5}$$

and the basis vectors are given by

$$\begin{aligned}
e_1^{\mathrm{T}}(x) &= \alpha_1[i \cos \pi i x_1 \sin \pi j x_2 \sin \pi k x_3, \; j \sin \pi i x_1 \cos \pi j x_2 \sin \pi k x_3, \\
&\qquad k \sin \pi i x_1 \sin \pi j x_2 \cos \pi k x_3] \\
e_2^{\mathrm{T}}(x) &= \alpha_2[-j \cos \pi i x_1 \sin \pi j x_2 \sin \pi k x_3, \; i \sin \pi i x_1 \cos \pi j x_2 \sin \pi k x_3, \; 0] \\
e_3^{\mathrm{T}}(x) &= \alpha_3[ik \cos \pi i x_1 \sin \pi j x_2 \sin \pi k x_3, \; jk \sin \pi i x_1 \cos \pi j x_2 \sin \pi k x_3, \\
&\qquad -(i^2 + j^2) \sin \pi i x_1 \sin \pi j x_2 \cos \pi k x_3]
\end{aligned} \tag{6}$$

where the i, j, k subscripts have been suppressed on e_n and α_n, and the coefficients $\alpha_{n,i,j,k}$ give each eigenvector unit energy. We will use the abbreviation ESBT to refer to this elastic-solid basis transformation. Notice that $h(x) = x - u(x)$ maps $\Omega = \mathbb{R}^3$ into Ω for equations (5) and (6). We make the assumption that both T and S are spatially band-limited to $[0, 1]^3$ so that $h(x)$ only needs to be evaluated on $[0, 1]^3$ and

not $\mathbb{R}^3$. We choose $\xi_{1,ijk}$, $\xi_{2,ijk}$ and $\xi_{3,ijk}$ to be zero-mean, independent Gaussian random variables with variances $\sigma_{1,i,j,k} = 2/(\pi^2(\lambda_0 + 2\mu_0)(i^2 + j^2 + k^2))$ and $\sigma_{2,i,j,k} = \sigma_{3,i,j,k} = 2/(\pi^2\mu_0(i^2 + j^2 + k^2))$, respectively. It can be shown that the potential of the elastic-solid model with the displacement field specified by (5) and (6) induces a Gaussian covariance structure on the coefficients $\xi = \{\xi_{n,i,j,k} : n = 1, 2, 3; i, j, k = 0, \ldots, N\}$. Notice that this parameterization of the displacement field corresponds to a Karhunen–Loeve expansion. It can also be shown that u corresponds to a band-limited quadratic-mean continuous Gaussian process. Note that a second basis can be constructed by replacing sines with cosines and cosines with sines in equation (6). This second basis has the advantage of mapping $\Omega = [0, 1]^3$ into Ω but suffers from the disadvantage of requiring T and S to be padded by background.

3.2. *Fluid model*

Transformations such as those based on the theory of elasticity develop restoring forces proportional to the deformed distance. Except for the smallest deformations, such elastic transformations prevent the textbook from being fully deformed into the shape of the patient's brain. The shortcomings of the elasticity model can be overcome by a viscous-fluid model, which allows the restoring forces to relax over time.

We take the approach described by Christensen *et al* (1993) to determine the viscous fluid spatial transformation (VFST). The VSFT at each time t satisfies the partial differential equation (PDE)

$$\mu\nabla^2 v + (\mu + \lambda)\nabla(\nabla^{\mathrm{T}} v) = b \tag{7}$$

where $v = [v_1(x, t), v_1(x, t), v_3(x, t)]^{\mathrm{T}}$ is the instantaneous velocity of the deformation field u. The gradient operator is defined by $\nabla = [\partial/\partial x_1, \partial/\partial x_2, \partial/\partial x_3]^{\mathrm{T}}$ and $\nabla^2 = \nabla^{\mathrm{T}}\nabla$ is the Laplacian. The body force b per unit volume is the discretization of the variational calculus gradient of (3). The $\nabla^2 v$ term in (7) is called the viscous term of the PDE. This term constrains neighbouring particles of the displacement field to deform with roughly the same velocity by spatially smoothing the velocity field. The $\nabla(\nabla^{\mathrm{T}} v)$ is called the mass source term and it allows structures in the textbook to grow and shrink in mass. The coefficients μ and λ are the viscosity coefficients.

An Eulerian reference frame is used to track the kinematics of the deformation. In this reference frame, a spatially fixed set of points—one located at each voxel in the study—is defined to observe the deformation of the textbook. As the textbook continuously deforms over time and space, points (particles) in the textbook flow through the observation points. At any instant of time, the transformation $h(x) = x - u(x)$ gives the original position of a particle as it passes through the observation point located at x. Since we are using an Eulerian reference frame, the velocity, v, of a particle is related to its displacement, u, by

$$v(x, t) = \partial u(x, t)/\partial t + v(x, t)^{\mathrm{T}}\nabla u(x, t). \tag{8}$$

The term $v(x, t)^{\mathrm{T}}\nabla u(x, t)$ accounts for the kinematic non-linearities of particles as they pass through the observation points.

4. Algorithms

4.1. *Minimum mean squared error estimation*

Minimum mean squared error (MMSE) estimation or conditional mean estimation is used to estimate the parameters of the ESBT. Samples of the posterior are generated by using the

stochastic differential equation (SDE)

$$\mathrm{d}\xi(t) = -\tfrac{1}{2}\nabla H(\xi(t))\,\mathrm{d}t + \mathrm{d}w(t) \tag{9}$$

where $w(t)$ is a vector-valued Wiener process with independent components and $H(\xi) = H(S, T) + H(u)$ is the Gibbs' potential of the posterior. Under appropriate conditions (Amit *et al* 1991, Grenander and Miller 1994), the sample mean generated from samples generated by the SDE converges to the conditional mean of the posterior, i.e.

$$\lim_{N\to\infty} \frac{1}{N}\sum_{i=1}^{N} \xi(t_i) = \int_{R^m} \xi\pi(\xi \mid S)\,\mathrm{d}\xi. \tag{10}$$

4.2. Time integration of viscous fluid PDE

The displacement field $\hat{u}$ satisfying the viscous fluid model is determined in the following manner. The time interval $[0, \infty)$ is discretized into small increments $0 = t_0 < t_1 < t_2 < \ldots$ and the displacement field at time t_0 for all $x \in \Omega$ is defined to be zero. Successive overrelaxation (SOR) with checker-board update (Strikwerda 1989) is used to solve (7) for the instantaneous velocity $v(x, t_i)$ of the displacement field at each point $x \in \Omega$. The SOR formula used for solving (7) in 2D at time t with grid spacing Δ is given by

$$\begin{aligned} v_{ij}^{(1)n+1} &= v_{ij}^{(1)n-1} + \omega((\Delta^2/6)(b_{ij}^{(1)} + 2v_{i+1j}^{(1)n-1} + 2v_{i-1,j}^{(1)n-1} + v_{ij+1}^{(1)n-1} + v_{ij-1}^{(1)n-1} \\ &\quad + \tfrac{1}{4}(v_{i+1,j+1}^{(2)n} + v_{i-1,j-1}^{(2)n} - v_{i+1,j-1}^{(2)n} - v_{i-1,j+1}^{(2)n})) - v_{ij}^{(1)n}) \\ v_{ij}^{(2)n+1} &= v_{ij}^{(2)n-1} + \omega((\Delta^2/6)(b_{ij}^{(2)} + 2v_{ij+1}^{(2)n-1} + 2v_{ij-1}^{(2)n-1} + v_{i+1j}^{(2)n-1} + v_{i-1j}^{(2)n-1} \\ &\quad + \tfrac{1}{4}(v_{i+1,j+1}^{(1)n} + v_{i-1,j-1}^{(1)n} - v_{i+1,j-1}^{(1)n} - v_{i-1,j+1}^{(1)n})) - v_{ij}^{(2)n}) \end{aligned} \tag{11}$$

where $\mu = 1$ and $\lambda = 0$ to simplify the notation. The subscripts ij denote the ijth pixel location in the study, the superscript n denotes the relaxation iteration, and the superscript (m) denotes the mth component of a vector. Through experimentation, $\omega = 1.5$ gives fast convergence of (11). Note that SOR is computationally intensive because it is an iterative algorithm. The displacement field at time t_{i+1} at each lattice point $x \in \Omega$ is determined from the instantaneous velocity at time t_i by

$$u(x, t_{i+1}) = u(x, t_i) + (t_{i+1} - t_i)(I - \nabla u(x, t_i)^{\mathrm{T}})v(x, t_i) \tag{12}$$

which is the discrete version of (8). Note that I is the identity matrix. The velocity of the displacement field and the value of the displacement field is calculated at each time point t_i and lattice point $x \in \Omega$ until the energy norm associated with the body force approaches zero (for a preset limit close to zero).

5. Experiments

The experiments were performed on a 64 × 64 DECmpp 12000Sx (MasPar) massively parallel, single-instruction multiple-data (SIMD) computer. This architecture is well suited for computing the transformations for three reasons. First, the computational power of the DECmpp is required to compute the 3D ESBT and VFST in a reasonable time. Second, the

nearest-neighbour interconnection between processors is very efficient for computing the SOR algorithm used to calculate the VFST. Finally, the global router and parallel indirect addressing of this computer—features not found on other mesh-connected computers—can efficiently fetch non-local data in order to transform the textbook.

The first experiment was designed to show how the ESBT and the VFST can be combined to generate a single transformation. For this experiment a 2D textbook was deformed into the 2D study using both the ESBT and the VFST. The W1 textbook and A1 study used in this experiment were constructed from spin-density, t1-weighted, and t2-weighted MR images that were collected in register by Scott Nadel of Duke University from two different subjects. The W1 textbook consisted of a spin-density, a t1-weighted, and a t2-weighted MR image of a single axial slice from the first subject and a hand segmentation that delineated the ventricles, head of the caudate nucleus, putamen, thalamus, other brain matter, and background. The t2 modality and the segmentation of the W1 textbook are shown in the left column of figure 1. The A1 study was constructed from corresponding spin-density, t1-weighted, and t2-weighted MR images of a single slice from the second subject. The slice used in the study was selected so that the study and the textbook contained the same structures. The t2 modality of the A1 study and a hand segmentation of this slice of the brain are shown in the middle column of figure 1. The right column of figure 1 shows the final transformation applied to the t2 modality and segmentation of the W1 textbook. Notice how similar the middle and right columns of figure 1 are.

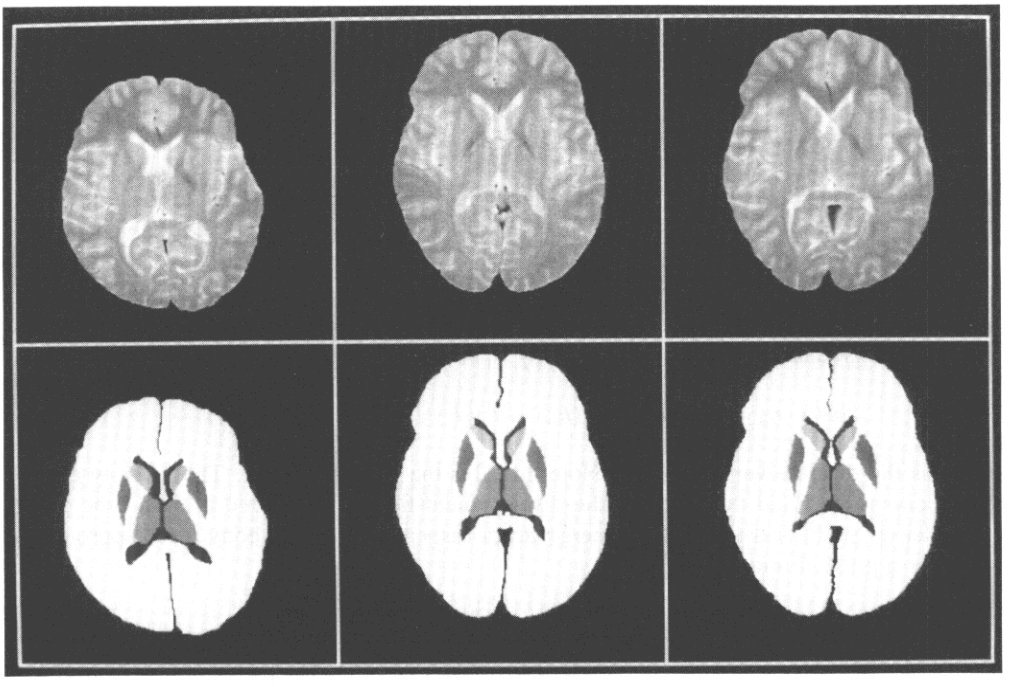

Figure 1. The left column shows the t2-weighted MR (top) and hand-drawn, nuclei segmentation (bottom) images from the W1 textbook. The middle column shows the t2-weighted MR (top) and hand-drawn, nuclei segmentation (bottom) images from the A1 study. The right column shows the result of deforming the W1 textbook t2-weighted MR (top) and segmentation (bottom) images into the shape of the A1 study.

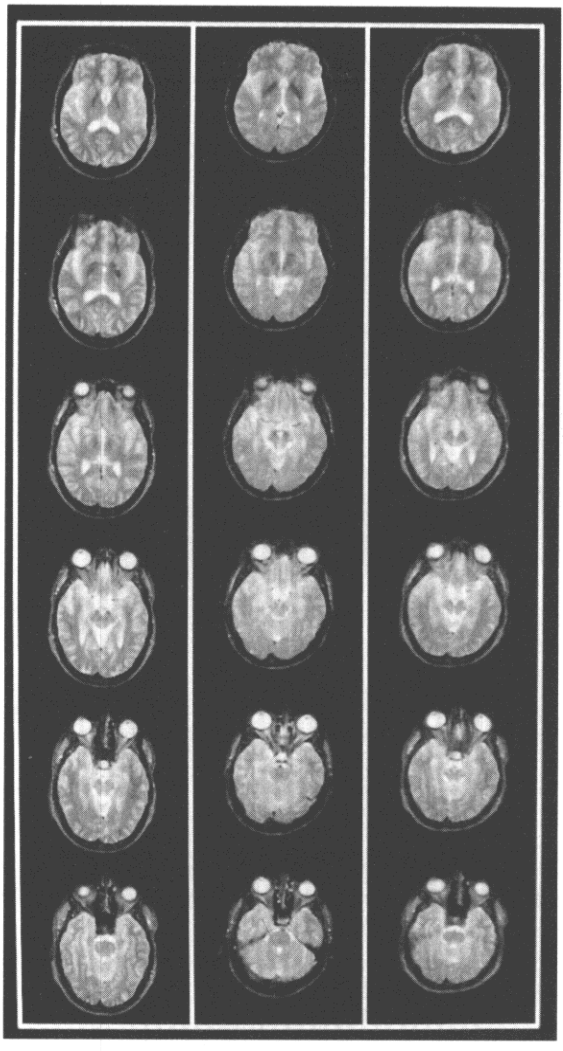

Figure 2. This figure shows slices 11–16 of the S1 textbook (left column), the D1 study (middle column), and the 3D ESBT deformed S1 textbook (right column) from top to bottom. Notice how similar the middle and right columns are. Also notice how the textbook deformed not only in the x and y directions, but also the z direction to match the study.

To avoid local minima when deforming the W1 textbook into the A1 study we took a multi-resolution approach. The idea is to match large structures first and then match smaller structures. The ESBT was estimated by running the SDE for 160 iterations. Initially, $d = 1$ in (5) and every 40 iterations d was incremented by one. The samples of the SDE for the last 20 iterations were averaged to generate the basis coefficients. The 3D elastic-solid basis was converted to a 2D basis as done by Miller *et al* (1993). As the number of basis functions increased, smaller and smaller variabilities between the textbook and study were accommodated. The ESBT took 134 s to estimate a 128×128 transformation. After estimating the ESBT, the VFST was estimated using the ESBT as an initial condition. The VFST was estimated in a coarse-to-fine manner by first estimating a 64×64 transformation

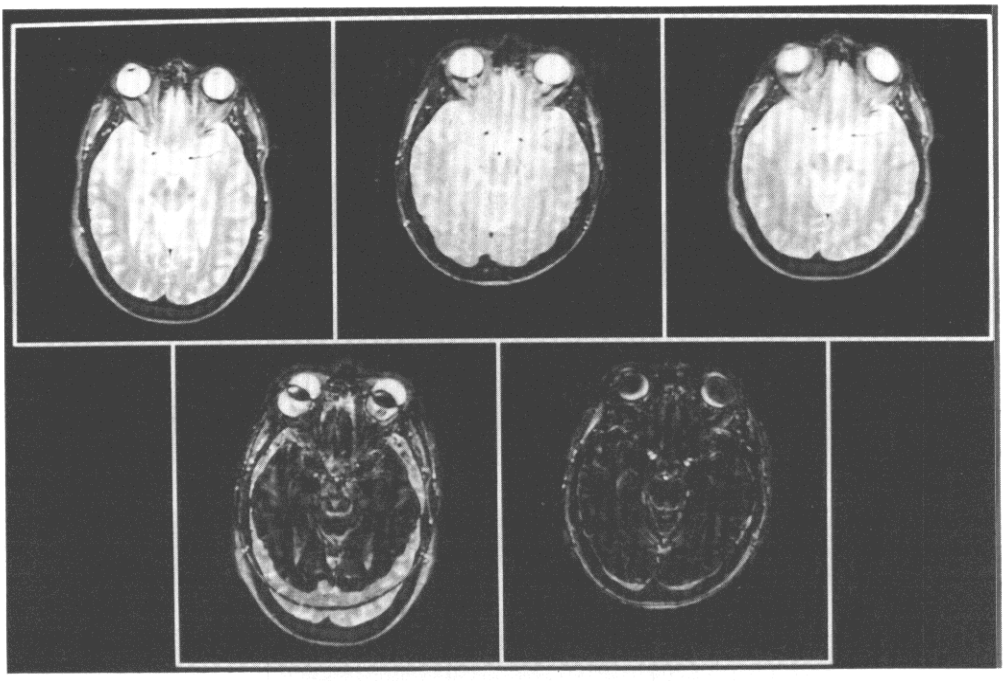

Figure 3. This figure shows slice 14 of the S1 textbook (top left) the D1 study (top middle) and the 3D ESBT deformed S1 textbook (top right). The difference images before transformation (left) and after transformation (right) are shown in the bottom row. Notice that the textbook slice had to deform in all three coordinate directions to match the study slice.

for 200 iterations using a 64×64 down-sampled version of the textbook and study. The VFST was then estimated at 128×128 for 40 iterations by up-sampling the 64×64 VFST and using a 128×128 down-sampled textbook and study. Finally, the 256×256 VFST was estimated by up-sampling the 128×128 VFST and using the 256×256 textbook and study. The execution time for the VFST is shown in table 1.

Table 1. Viscous fluid transformation times (DECmpp 12000Sx).

Image size	Number of PDE iterations	Number of time steps	Time (s)	Total time (s)
64×64	250	200	33	
128×128	250	40	27	85.3
256×256	250	8	24	

Table 2 shows the relative overlap of all the segmented regions before transformation, after application of the ESBT, and after application of the VFST. The relative overlap measure was first introduced by Dann *et al* (1989) and is a useful measure for comparing two different segmentations when neither is necessarily correct. The relative overlap of a structure is defined to be the area of the intersection of structure in both segmentations divided by the area of their union. This table shows that the relative overlap increased for each of the structures after applying the ESBT and again after applying the VFST. Notice that the head

Table 2. Relative overlap for experiment 1.

Structure	Before transformation	After elastic-solid basis transformation	After fluid transformation
Background	0.79	0.96	0.99
Ventricles	0.017	0.43	0.63
Thalamus	0.097	0.64	0.81
Head of caudate nucleus	0.0	0.53	0.78
Putamen	0.0	0.45	0.70
Other brain matter	0.53	0.86	0.95

of the caudate nucleus did not overlap initially in the textbook and study, but had a relative overlap of 0.78 after transformation. Also, the relative overlap of the background went from 0.79 to 0.99, which means that the outer contour of the deformed textbook matched almost perfectly with the outer contour of the study.

To demonstrate the procedure in 3D, Marcus Raichle and Tom Videen of Washington University collected 21 consecutive, t2-weighted MR slices with 5 mm spacing from a schizophrenic patient and a depressed patient. A 3D textbook was constructed using the images from the schizophrenic patient and a 3D study was constructed using the images from the depressed patient. The choice of study and textbook was arbitrary. This textbook and study will be referred to as the S1 textbook and the D1 study. For computation, the two volumes were reduced from $256 \times 256 \times 21$ voxels to $64 \times 64 \times 21$ voxels by averaging 4×4 blocks of voxels in each slice of the volume. The transformation was estimated in 251 s. After determining the coefficients for the $64 \times 64 \times 21$ ESBT, the ESBT was applied to the full $256 \times 256 \times 21$ voxel textbook. Figure 2 shows slices 11–16 of the S1 textbook (left column), the D1 study (middle column), and the 3D ESBT deformed S1 textbook (right column) from top to bottom. Notice how similar the middle and right columns are. Also notice how the textbook deformed not only in the x and y directions, but also the z direction to match the study. Figure 3 shows slice 14 of the S1 textbook (top left) the D1 study (top middle), and the 3D ESBT deformed S1 textbook (top right). The bottom row shows the difference images between slice 14 of the study and the textbook before transformation (left) and after transformation (right). Notice that the ventricles in slice 14 of the textbook do not appear in slice 14 of the study. To accommodate this difference the ventricles have been translated in the axial direction so they do not appear in slice 14 of the deformed textbook.

Acknowledgments

We are indebted to Marcus Raichle and Tom Videen of Washington University and Scott Nadel of Duke University for supplying us with data. This work is supported by the NIH-NCRR-RR01380, ONR N00014-92-J-1418, ARO P-29349-MA-SDI, and a grant from the Digital Equipment Corporation.

References

Amit Y, Grenander U and Piccioni M 1991 Structural image restoration through deformable templates *J. Am. Stat. Assoc.* **86** 376–87

Bajcsy R and Kovacic S 1989 Multiresolution elastic matching *Comput. Vision, Graphics Image Proc.* **46** 1–21

Christensen G E, Rabbitt R D and Miller M I 1993 A deformable neuroanatomy textbook based on viscous fluid mechanics *Proc. 27th Annual Conf. on Information Science and Systems (Baltimore, 1993)* ed J Prince and T Runolfsson (Baltimore, MD: John Hopkins University) pp 211–6

Collins D L, Peters T M, Dai W and Evans A C 1992 Model-based segmentation of individual brain structures from MRI data *Visualization in Biomedical Computing 1992* vol 1808, ed R A Robb (Bellingham, WA: SPIE) pp 10–23

Dann R, Hoford J, Kovacic S, Reivich M and Bajcsy R 1989 Evaluation of elastic matching systems for anatomic (CT, MR) and functional (PET) cerebral images *J. Comput. Assist. Tomogr.* **13** 603–11

Evans A C, Dai W, Collins L, Neelin P and Marret S 1991 Warping of a computerized 3-D atlas to match brain image volumes for quantitative neuroanatomical and functional analysis *Image Process.* **1445** 236–46

Grenander U and Miller M I 1994 Representations of knowledge in complex systems *J. Royal Stat. Soc.* B **56**

Miller M I, Christensen G E, Amit Y and Grenander U 1993 Mathematical textbook of deformable neuroanatomies *Proc. Natl. Acad. Sci. USA* **90** 11 944–8

Pelizzari C A, Chen G T Y, Spelbring D R, Weichselbaum R R and Chen C T 1989 Accurate three-dimensional registration of CT, PET, and/or MR images of the brain *J. Comput. Assist. Tomogr.* **13** 20–6

Strikwerda J 1989 *Finite Difference Schemes and Partial Differential Equations* (Pacific Grove: Wadsworth and Brooks/Cole)